JGR Space Physics

RESEARCH ARTICLE
10.1029/2019JA026713

Characteristics of GNSS Total Electron Content Enhancements Over the Midlatitudes During a Geomagnetic Storm on 7 and 8 November 2004

T. Sori[1], A. Shinbori[1], Y. Otsuka[1], T. Tsugawa[2], and M. Nishioka[2]

[1]Institute for Space-Earth Environmental Research (ISEE), Nagoya University, Nagoya, Japan, [2]National Institute of Information and Communications Technology (NICT), Tokyo, Japan

Key Points:
- TEC enhancements first appeared in the middle-latitude regions associated with the geomagnetic storm
- The TEC enhancement observed in Japan appeared with a magnetic conjugacy in the Southern Hemisphere
- TEC enhancements in the afternoon to night sectors were simultaneously observed within a wide longitudinal width (~100°)

Correspondence to:
T. Sori,
sori.takuya@isee.nagoya-u.ac.jp

Citation:
Sori, T., Shinbori, A., Otsuka, Y., Tsugawa, T., & Nishioka, M. (2019). Characteristics of GNSS total electron content enhancements over the midlatitudes during a geomagnetic storm on 7 and 8 November 2004. *Journal of Geophysical Research: Space Physics*, *124*, 10,376–10,394. https://doi.org/10.1029/2019JA026713

Received 11 MAR 2019
Accepted 27 AUG 2019
Accepted article online 10 OCT 2019
Published online 04 DEC 2019

Abstract The characteristics of global electron density variations in the ionosphere during a geomagnetic storm on 7 and 8 November 2004 were investigated using total electron content (TEC) obtained from the global navigation satellite system (GNSS). The regions of enhanced TEC over North America, Europe, and Japan first appeared in the middle-latitude regions. The TEC enhancements over North America showed a rapid longitudinal expansion and reached a wide longitudinal extent during the initial and main phases of the geomagnetic storm. TEC enhancements were simultaneously observed in both North America and Japan at 05:00 UT on 8 November. Observation data from the Defense Meteorological Satellite Program showed a slight enhancement of electron density at 850 km below the equatorward boundary of the middle-latitude trough (45–48°N in geomagnetic latitude) over the Pacific Ocean. This electron density variation may correspond to the TEC enhancements observed in both Japan and North America. These results imply that an enhanced TEC region existed between North America and Japan. The TEC enhancement in Japan appeared with a magnetic conjugacy in the Southern Hemisphere, indicating one of the characteristics of storm-enhanced density (SED). Moreover, TEC enhancements simultaneously appeared from Japan to central Asia at 11:00 UT on 8 November, corresponding to the early recovery phase of the geomagnetic storm. From the above results, it is suggested that SED phenomena can be simultaneously generated over a wide longitudinal width (~100°). The longitudinal extent of this SED event is 2.5–5.0 times longer than those reported by previous studies.

1. Introduction

As electron density distribution in the ionosphere is mainly determined by a balance between ionization of the upper atmosphere by solar extreme ultraviolet radiation and recombination of ionospheric plasmas with neutral particles, it shows clear variations with local time, latitude, and longitude, reflecting significant enhancement in sunlit regions. The ionospheric electron density shows significant increases or decreases on a global scale associated with geomagnetic storms (e.g., Matsushita, 1959; Matuura, 1972; Buonsanto, 1999). During the early main phase of a geomagnetic storm, a positive ionospheric storm showing an enhancement of the electron density in low latitudes is caused by the equatorward thermospheric wind (e.g., Lin et al., 2005; Balan et al., 2009; 2010), in addition to the storm time eastward penetrating electric field (e.g., Kelley et al., 2004; Tsurutani et al., 2004). These physical processes play an important role in the manifestation of an equatorial ionization anomaly (EIA). During the recovery phase of a geomagnetic storm, a negative ionospheric storm showing a depression in the electron density occurs in association with a change in the neutral composition ratio (O/N_2) (e.g., Fagundes et al., 2016). Such global changes in the ionospheric electron density during geomagnetic storms can be easily seen in a two-dimensional map of total electron content (TEC). The detailed characteristics of ionospheric storms and their generation mechanism have been reviewed by many papers (e.g., Abdu, 1997; Buonsanto, 1999; Fuller-Rowell et al., 1997; Prölss, 1997; Rees, 1996; Schunk & Sojka, 1996).

The high-density ionospheric plasma in the afternoon sector can be transported from middle and low latitudes to the cusp/cleft region by the storm time-enhanced convection electric field. This storm-enhanced density (SED; Foster, 1993) becomes a source for an enhanced tongue of ionization in the polar cap (Liu

et al., 2016b) and also contributes to the middle-latitude ionospheric storm (Thomas et al., 2013). The primary features of the SED phenomenon include a latitudinally narrow structure of the plasma density with westward and poleward convection, high electron density, an elevated *F* region peak, a significantly enhanced topside ionosphere, and low electron temperatures near sunset in the midlatitudes (Liu et al., 2015, 2016a). Foster and Rideout (2007) reported that an SED plume frequently occurs in magnetically conjugate regions in both the Northern and Southern Hemispheres, and the poleward edge of the SED plume is almost closely conjugate. The SED phenomenon has been observed in North America (e.g., Foster, 1993; Coster et al., 2007; Basu et al., 2008), Japan (Maruyama, 2006), Europe (Yizengaw et al., 2006), and South America (Coster et al., 2003).

Recent studies on the generation mechanism of the SED plume have shown that westward plasma transport associated with an enhanced subauroral polarization stream (SAPS; Foster and Vo, 2002) mainly contributes to SED plume formation in the low- and middle-latitude ionosphere (Foster et al., 2007). The upwelling effects of ionospheric plasma via penetration of the electric field into the middle- and low-latitude ionosphere (Spiro et al., 1988) and equatorward thermospheric winds (Fuller-Rowell et al., 1994) have also been proposed as candidates for the SED generation mechanism. Liu et al. (2016b) compared two geomagnetic storm events occurring on 17 March 2013 and 2015, using the Thermosphere Ionosphere Electrodynamic General Circulation Model and GPS-TEC observations to identify the principal SED mechanisms. They concluded that local upward $\mathbf{E} \times \mathbf{B}$ ion drifts are the most important factor in SED formation in the topside ionosphere, while neutral winds play a major role in generating SEDs in the bottomside *F* region ionosphere.

Many previous works have been published on the temporal and spatial evolution of the ionosphere during two intense geomagnetic storms that occurred on 7–12 November 2004. Using GPS-TEC data over Japan within a geographic latitudinal range of 27°N to 45°N from the GPS Earth Observation Network, Maruyama (2006) reported that an anomalous TEC enhancement appeared at higher latitude (~45°N) in Japan during the early recovery phase of the first geomagnetic storm that occurred on 7 and 8 November 2004. He noted that the middle-latitude TEC enhancement observed after sunset was related to the SED plume with a westward velocity of 8°/hr. Dashora and Pandey (2007) reported on the ionospheric variations near the crest of the EIA during the first geomagnetic storm using GPS-TEC and ionosonde data in the Indian sector. They showed that the disturbance dynamo fields inhibited the equatorial plasma fountain effect and caused a reduction in TEC in India on 8 November. Fejer et al. (2007) investigated the equatorial ionospheric electric fields using radar measurements from the Jicamarca Radio Observatory, magnetometer observations from the Pacific sector, and ionosonde data from Brazil during the two geomagnetic storms on 7–12 November 2004. They observed large and rapidly varying eastward and westward electrojet perturbations in the daytime over Jicamarca during the main phase of the geomagnetic storm on 7 November 2004 despite the nearly steady polar cap potential and southward interplanetary magnetic field (IMF). They also found that the largest daytime prompt penetration electric fields (about 3 mV/m) over Jicamarca were observed during the main phase of the second geomagnetic storm on 9 November 2004. Balan et al. (2009) investigated the relative importance of electric field and neutral wind using GPS-TEC, peak electron density, and modeling at low-middle latitudes in the longitude range around Japan during the two geomagnetic storms on 7–11 November 2004. They concluded that the equatorward winds produced stronger positive ionospheric storms without a penetrating eastward electric field than they did with a penetrating eastward electric field. Simi et al. (2013) also showed the ionospheric response at the equatorial and near-equatorial regions in the Indian sector during the geomagnetic storms on 8–10 November 2004. They used ionosonde, magnetic field, and Global Ultraviolet Imager (GUVI) O/N_2 data and revealed the important role of storm-induced O/N_2 changes, along with prompt penetration electric fields and disturbance dynamo electric fields in modulating the ionization distribution in the EIA region during this geomagnetic storm. However, because most previous studies have focused on temporal and spatial variations in TEC within a specific region and the time and spatial resolutions of the data were not sufficiently high, the detailed features of global TEC variation associated with the development and decay of a geomagnetic storm have not yet been clarified. The purpose of this study is to investigate the characteristics of global ionospheric variations during the first geomagnetic storm on 7 and 8 November 2004, using global GNSS-TEC data with high temporal and spatial resolution, and to understand the generation mechanism of storm time TEC enhancement in the middle-latitude ionosphere related to SED phenomena.

2. Data sets and Analysis Method

2.1. Data Sources and TEC Data Processing

To derive global GNSS-TEC data, we first collected a large number of receiver independent exchange formatted files obtained from many regional GNSS receiver networks after 1988. The number of GNSS stations reached more than 8,500 in January 2019. These receiver independent exchange files were provided by the International Geoscience Services (ftp://igs.ensg.ign.fr/pub/igs/data), University NAVSTAR Consortium (ftp://data-out.unavco.org/pub/rinex/obs), Crustal Dynamics Data Information System (ftp://cddis.gsfc.nasa.gov/pub/gps/data/daily), Scripps Orbit and Permanent Array Center (ftp://garner.ucsd.edu/pub/rinex), Reseau National GPS permanent (ftp://renag.unice.fr/data), Système d'Observation du Niveau des Eaux Littorales (ftp://ftp.sonel.org/gps/data), TrigNet Web Application in South Africa (ftp://ftp.trignet.co.za), Instituto Brasileiro de Geografia e Estatística (ftp://geoftp.ibge.gov.br/informacoes_sobre_posicionamento_geodesico/ rbmc/dados), SWEPOS–Sweden (ftp://ftp-sweposdata.lm.se:21/Rinex-data/Rinex2/se_swepos_daily), Norwegian Mapping Authority (ftp://ftp.statkart.no/rnx2/24hour/30sec, user ID and password are required for access to the data), Can-Net Virtual Reference Station Network (ftp://gpsweb.cannet.ca/RINEX), and other global and regional data centers (a total of more than 50 data providers) (Shinbori et al., 2018).

As a second step, we calculated the TEC from the difference in the two carrier Phases L1 and L2, at a radio frequency of 1,575.42 and 1,227.60 MHz, respectively, associated with propagation into the ionosphere. Although we can also derive TEC data from the difference in two pseudoranges (P1 and P2), the accuracy of the difference in the two carrier phases is 2 orders of magnitude higher than the TEC value calculated using the difference in two pseudoranges (Jakowski et al., 1996). The TEC data derived from the difference in L1 and L2 are relative values of TEC because of integer cycle ambiguities and instrumental biases. The cycle ambiguities can be excluded by using corresponding TEC values calculated from the pseudoranges at dual frequencies, but the instrumental biases remain unknown. Therefore, we needed to estimate these biases to determine the absolute TEC values.

To estimate the instrumental biases, Otsuka et al. (2002) have proposed a method that consists of two steps. In this study, the instrumental biases were calculated in the first step, in which hourly averaged absolute TEC values and instrumental biases were calculated using a weighted least squares fitting method. Then, the absolute TEC with a time resolution of 30 s was obtained by subtracting the calculated instrumental biases from the original TEC. Detailed information regarding this procedure can be found in Otsuka et al. (2002). Because the absolute TEC data derived using this method are integrated values in the line-of-sight direction between the GPS satellite and receiver, we converted the slanted TEC values into corresponding vertical values, assuming a thin-shell ionosphere at an altitude of 300 km. Moreover, we specified a maximum satellite zenith angle of 75° and created a data grid of the absolute TEC with a time and spatial resolution of 30 s and 0.5° × 0.5° in longitude and latitude, respectively. The GNSS-TEC data are stored in a database managed by the Dense Regional and Worldwide International GNSS-TEC observation (DRAWING-TEC) project (http://seg-web.nict.go.jp/GPS/DRAWING-TEC/) at NICT (Tsugawa et al., 2007, 2018). In this study, we finally analyzed every 5-min interval of GNSS-TEC data at the same spatial resolution to investigate the temporal and spatial variations of global GNSS-TEC during the geomagnetic storm.

To investigate variations in the solar wind, IMF, and geomagnetic indexes (AE and SYM-H) during the geomagnetic storm that occurred on 7 and 8 November 2004, we used high-resolution OMNI data provided by Coordinated Data Analysis Web (CDAWeb) and National Aeronautics and Space Administration (https://cdaweb.sci.gsfc.nasa.gov/index/.html) and the AE and SYM-H indexes provided by the World Data Center for Geomagnetism, Kyoto University (https://wdc.kugi.kyoto-u.ac.jp). We also referred to a list of geomagnetically quiet and disturbed days provided by the World Data Center for Geomagnetism, Kyoto University, to calculate the average GNSS-TEC values for 10 geomagnetically quiet days in November 2004. The criteria for geomagnetically quiet days and disturbed days are found in the webpage (https://www.gfz-potsdam.de/en/kp-index/). The quietest days and most disturbed days of each month were selected by their Kp indices on the basis of three criteria for each day: (1) the sum of the eight Kp values, (2) the sum of squares of the eight Kp values, and (3) the maximum of the eight Kp values. According to each of the above criteria, a relative order number is assigned to each day of the month, the three-order numbers are

averaged, and the days with the lowest and the highest mean order numbers are selected as the five (respectively 10) quietest and the five most disturbed days. We also used electron temperature, density, and horizontal ion drift data obtained from the Special Sensor-Ions, Electrons, and Scintillation Microprocessor and the Special Sensor-Ions, Electrons, and Scintillation Driftmeter onboard Defense Meteorological Satellite Program (DMSP) satellites provided by the National Oceanic and Atmospheric Administration (https://satdat.ngdc.noaa.gov/dmsp/) for a comparison between the GNSS-TEC data and electron density variations. The DMSP satellites fly in Sun-synchronous near-polar orbits at an altitude of 850 km with an orbital period of approximately 100 min. We further used the GUVI O/N_2 ratio data provided by a website (http://guvitimed.jhuapl.edu/) to investigate the global distribution of the neutral composition ratio during the geomagnetic storm. Furthermore, we used thermospheric wind data recorded by the Fabry-Perot interferometer (FPI) at Shigaraki (http://stdb2.isee.nagoya-u.ac.jp/omti/data/data.html). Detailed information regarding the FPI at Shigaraki can be found in Shiokawa et al. (2003).

2.2. Analysis Method

To obtain the quiet time average TEC data, we first calculated the average TEC of 10 geomagnetically quiet days during November 2004, referring to the list of geomagnetically quiet days and disturbed days. As a second step, to identify the global GNSS-TEC variations associated with the development and decay of the geomagnetic storm that occurred on 7 and 8 November 2004, we calculated the absolute TEC difference (dTEC) between the storm time TEC and average TEC of 10 geomagnetically quiet days during November 2004. A detailed description of the method used to derive the dTEC values can be found in Shinbori et al. (2018). As a third step, we normalized the dTEC values by the absolute value of the average TEC of 10 geomagnetically quiet days and defined it as the ratio of the TEC difference (rTEC). Using the rTEC data, we created a two-dimensional map of rTEC in geographic and geomagnetic coordinates. In converting the GNSS-TEC data into geomagnetic coordinates at a height of 300 km, we used the Altitude-Adjusted Corrected GeoMagnetic model (Shepherd, 2014). To identify the magnetic conjugacy of the storm time GNSS-TEC variation in both hemispheres, we obtained the magnetic conjugate points from a website (https://omniweb.gsfc.nasa.gov/vitmo/cgm.html) to run the International Geomagnetic Reference Field-12 model (Thebault et al., 2015). In these analyses, we used data analysis software (Tanaka et al., 2013) developed by the Inter-university Upper atmosphere Global Observation NETwork project (Hayashi et al., 2013).

3. Results

3.1. Geomagnetic Conditions

Figure 1 shows an overview of the geomagnetic storm that occurred on 7 and 8 November 2004. As shown in Figure 1a, the solar wind flow speed increased from 330 to 750 km/s with several step-like variations at 03:00, 11:00, and 18:45 UT on 7 November 2004. The speed reached a maximum at 05:00 UT on 8 November 2004. These step-like increases of the solar wind flow speed correspond to sudden increases in the SYM-H value as shown in Figure 1d. This signature of the SYM-H index shows a sudden commencement or impulse caused by the dayside magnetopause current because of the arrival of a solar wind shock or discontinuity. These negative variations indicate the development of a ring current in the inner magnetosphere because of the strong convection electric field due to a reconnection process between the southward IMF and the Earth's magnetic field (Tsurutani et al., 2006). As shown in Figure 1b, the IMF Bz was directed southward during 15:00–17:00 and 20:00–22:00 UT on 7 November and 23:00–12:00 UT on 7 and 8 November. Corresponding to these periods, the SYM-H index showed a significant decrease and reached a minimum value of −400 nT at 06:00 UT on 8 November, as shown in Figure 1d. As shown in Figure 1c, many sudden enhancements of the AE value were seen during the storm period on 7 and 8 November 2004; the maximum value was ~3,000 nT at 10:00 UT on 8 November.

3.2. Characteristics of the Storm Time Global TEC Variations

3.2.1. Initial Phase

Figures 2b–2i show a two-dimensional global map of rTEC as a function of geographical longitude and latitude during 12:00–19:00 UT on 7 November 2004. The dotted curves and the numbers at 180°E indicate the magnetic latitude at a height of 300 km calculated using the Altitude-Adjusted Corrected GeoMagnetic model. As shown in Figures 2d–2f, an enhancement of rTEC appeared in the high-latitude region (~60°N) of Europe at 14:00 UT on 7 November and expanded into the low-latitude region with time. In Figures 2f

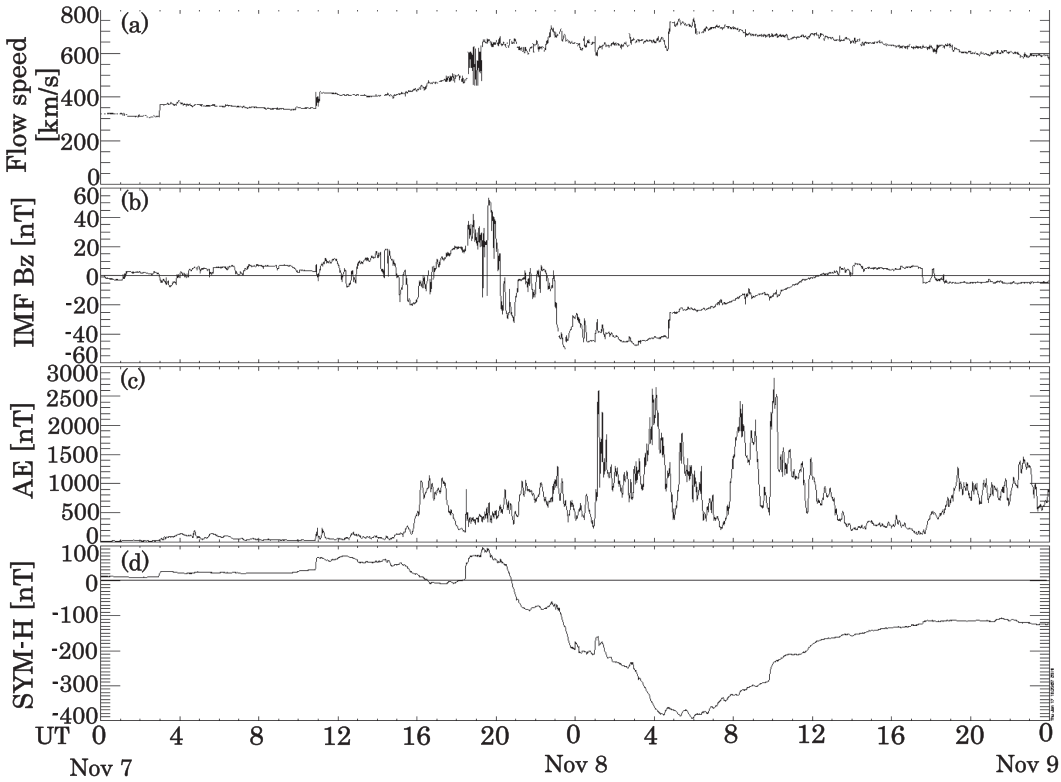

Figure 1. Time series plots of (a) flow speed, (b) IMF Bz, (c) AE, and (d) SYM-H in a time interval between 7 and 8 November 2004. IMF = interplanetary magnetic field.

and 2g, another enhancement of rTEC appeared in the high-latitude region (~45°N) of North America at 16:00 UT on 7 November and rapidly expanded in the longitudinal direction within 1 hr. After that, the enhanced rTEC region also slowly expanded into the low-latitude region (Figures 2g–2i). It is noted that the rTEC values in the equatorial and low-latitude regions did not show a significant change during 16:00–19:00 UT on 7 November.

3.2.2. Main Phase

Figures 3b–3i show a two-dimensional global map of rTEC as a function of geographical longitude and latitude during 20:00–03:00 UT on 7 and 8 November. The color code indicates rTEC values from −1 to 2. As shown in Figures 3b and 3c, a region of enhanced rTEC appeared in the high-latitude region of North America at 20:00 UT on 7 November and expanded rapidly in the longitudinal direction within 1 hr. As shown in Figures 3d–3i, the enhanced rTEC region expanded into the low-latitude region with the development of the geomagnetic storm. A region of decreased rTEC with a narrow latitudinal structure can be clearly seen above the latitude of the enhanced rTEC region, corresponding to the middle-latitude trough. Its location also moved equatorward with time. On the other hand, another rTEC enhancement region began to appear in the low-latitude region (~30°N) of the east side of Japan and extended westward within several hours, as shown in Figures 3e–3i.

3.2.3. Recovery Phase

Figures 4b–4i show a two-dimensional global map of rTEC as a function of geographical longitude and latitude during 04:00–11:00 UT on 8 November. The color code indicates rTEC values from −1 to 6. As shown in Figure 4c, the rTEC enhancement associated with the equatorward motion of the middle-latitude trough can be seen in the low-latitude region (~20°N) of North America and another rTEC enhancement region began to appear in the high-latitude region (~45°N) of Japan at 05:00 UT on 8 November. After 06:00 UT, a large rTEC enhancement region appeared over Japan (35–45°N; Figures 4d–4i). Moreover, rTEC enhancement can also be seen in the Southern Hemisphere (from −35°N to −15°N and 130°E to 170°E in geographic latitude and longitude, respectively). However, the average value of rTEC fell within a range of 2.5–3.0 and was

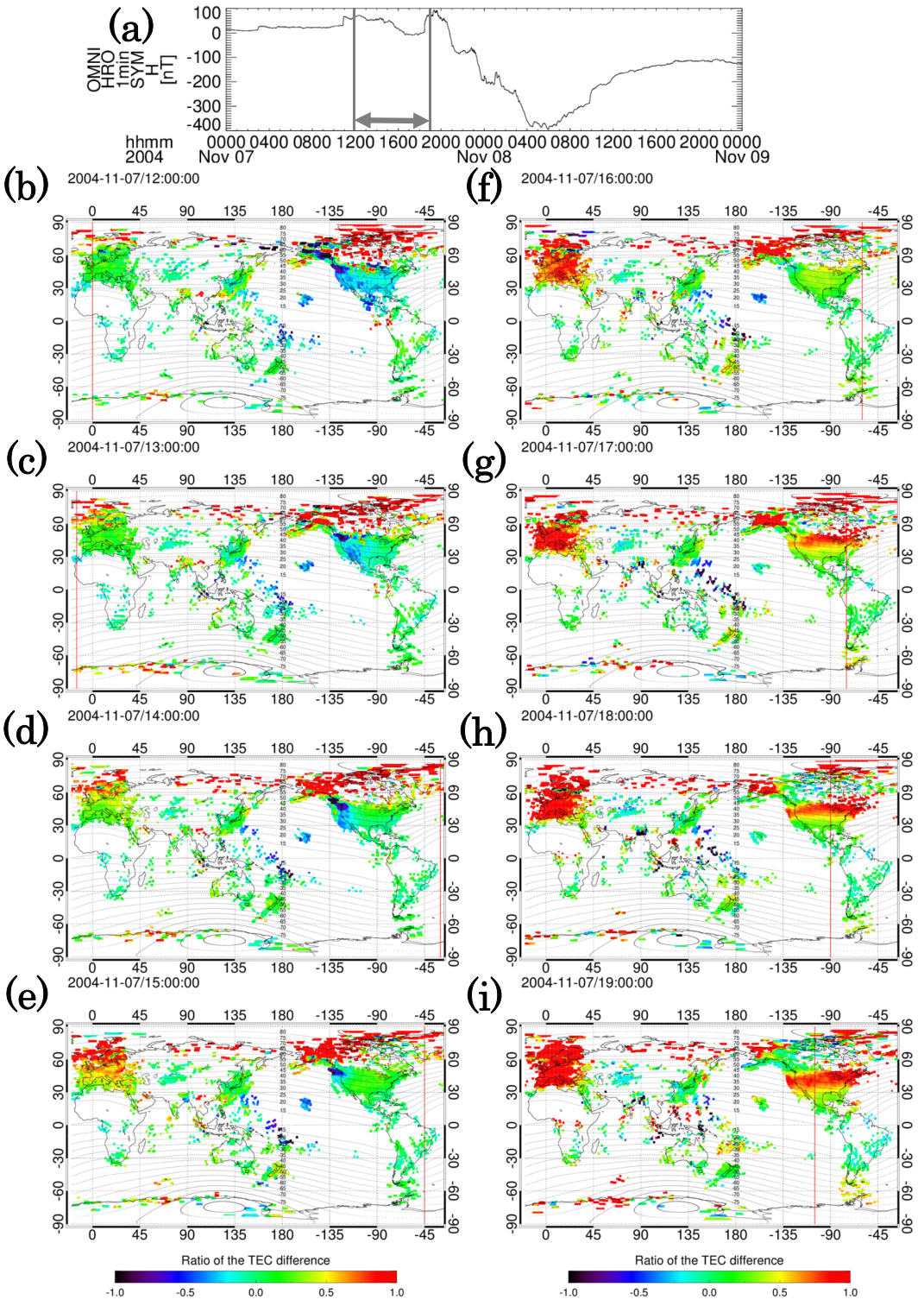

Figure 2. Time series plot of (a) SYM-H. (b)–(i) Two-dimensional world maps of rTEC at 1-hr intervals during 12:00–19:00 UT on 7 November 2004, corresponding to the initial phase of the geomagnetic storm. The color code indicates the rTEC value within a range of −1 to 1. The vertical red line represents local noon. The horizontal arrow indicates the period of the two-dimensional rTEC maps. TEC = total electron content.

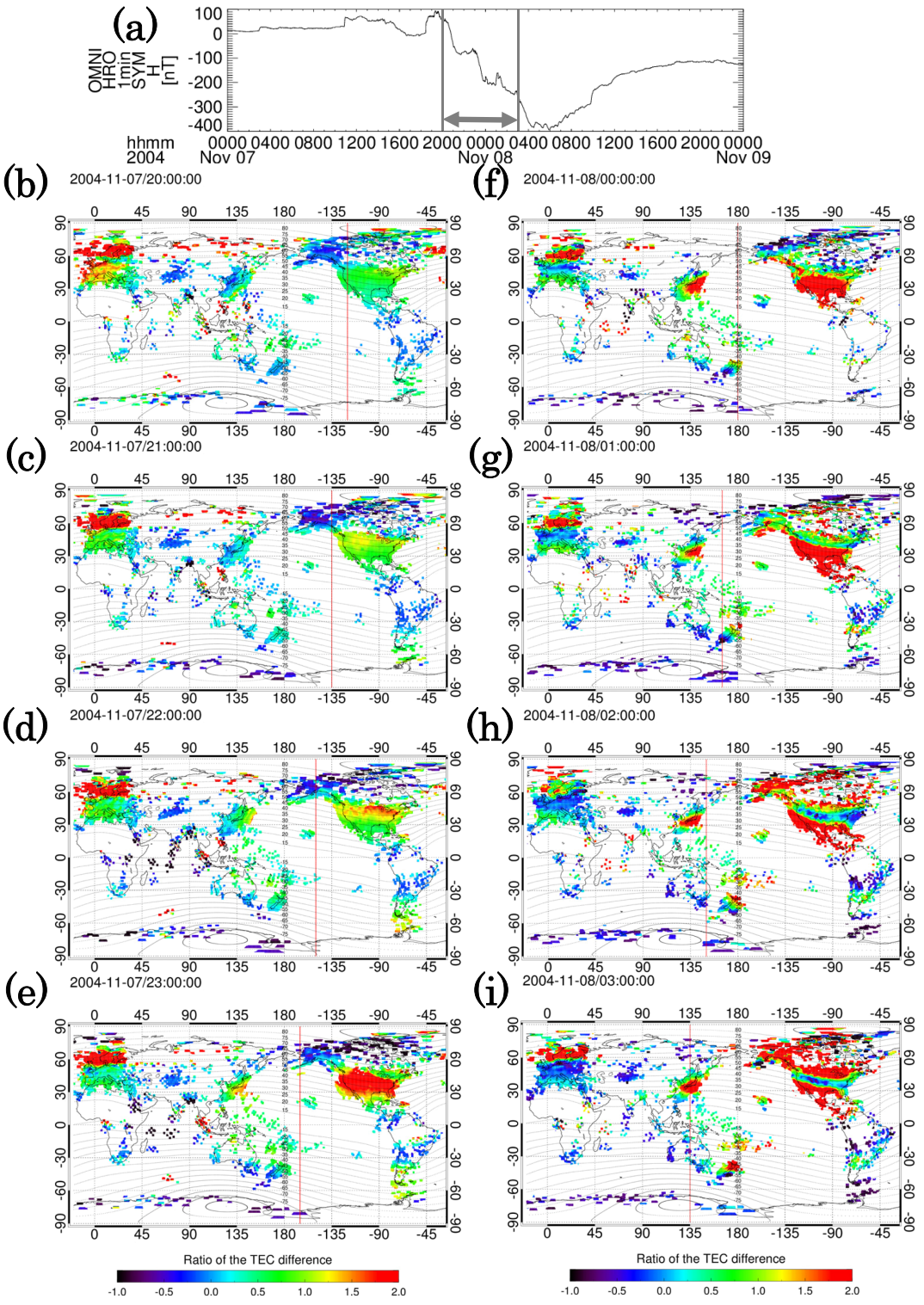

Figure 3. Time series plot of (a) SYM-H. (b)–(i) Two-dimensional world maps of rTEC at 1-hr intervals during 20:00–03:00 UT on 7 and 8 November 2004, corresponding to the main phase of the geomagnetic storm. The color code indicates the rTEC value within a range of −1 to 2. The vertical red line represents local noon. The horizontal arrow indicates the period of the two-dimensional rTEC maps. TEC = total electron content.

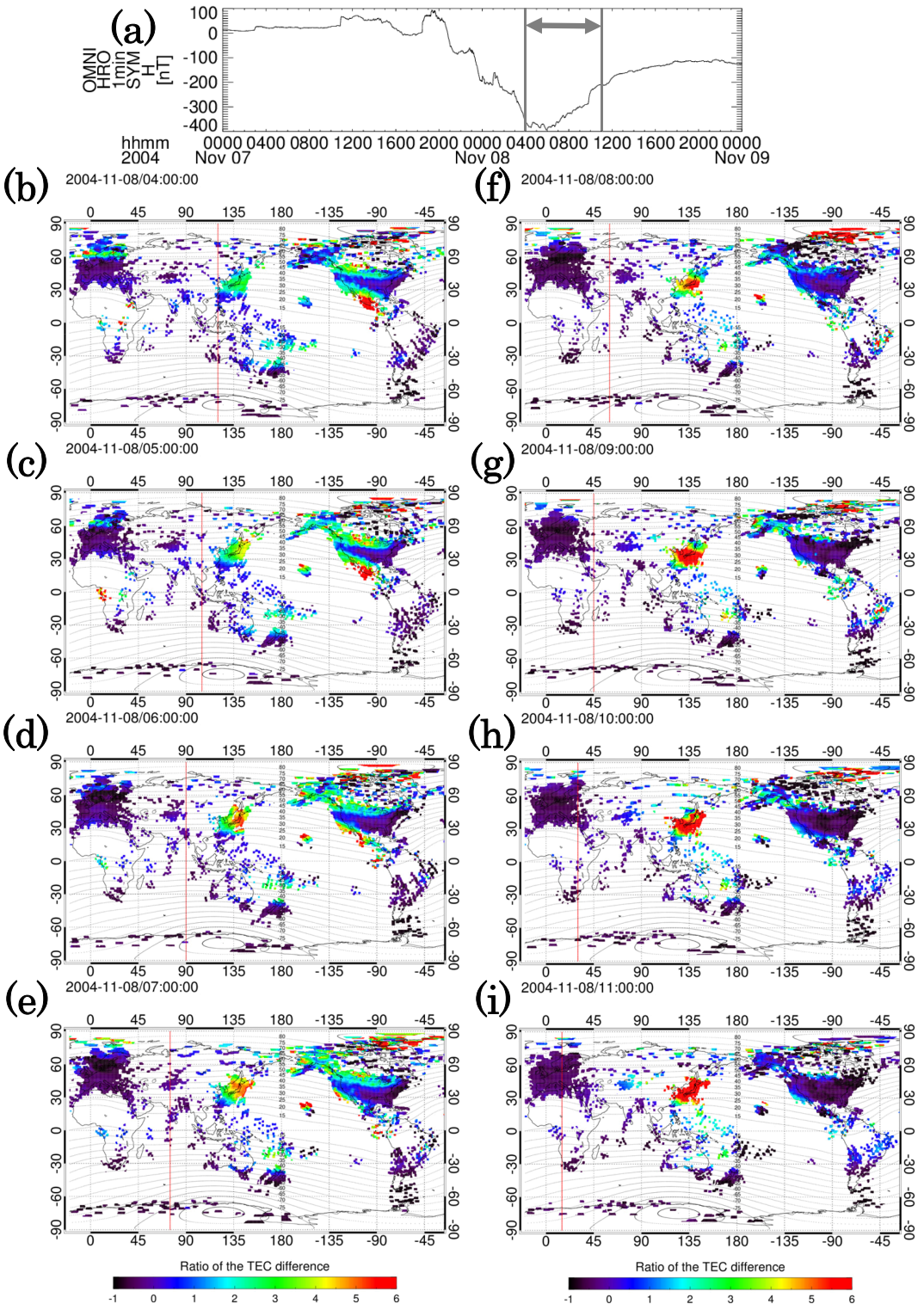

Figure 4. Time series plot of (a) SYM-H. (b)–(i) Two-dimensional world maps of rTEC at 1-hr intervals during 20:00–03:00 UT on 7 and 8 November 2004, corresponding to the recovery phase of the geomagnetic storm. The color code indicates the rTEC value within a range of −1 to 6. The vertical red line represents local noon. The horizontal arrow indicates the period of the two-dimensional rTEC maps. TEC = total electron content.

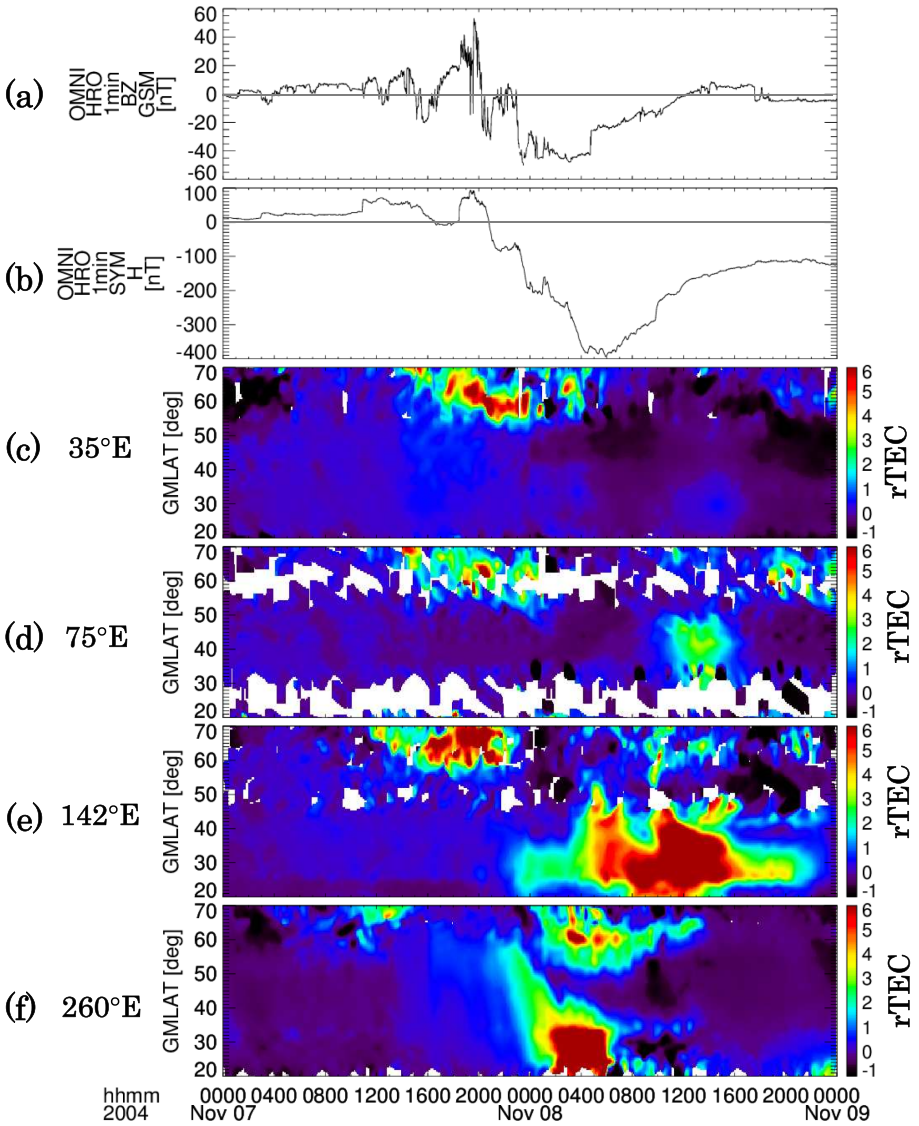

Figure 5. Time series plots of (a) interplanetary magnetic field Bz and (b) SYM-H and GMLAT-time plots of rTEC (c) at 35°E, (d) at 75°E, (e) at 142°E, and (f) at 260°E on 7 and 8 November 2004. The color bars in (c)–(f) indicate rTEC values within a range of -1 to 6. TEC = total electron content.

much smaller in the Southern Hemisphere than in Japan. Moreover, the rTEC values in other regions (Europe and North and South America) were less than 1.5 during the recovery phase of the geomagnetic storm. Detailed features of global rTEC variation during the geomagnetic storm will be described later.

3.3. Geomagnetic Latitudinal Distribution of the Storm Time Global TEC Variations

Figure 5 shows the time series plots of the IMF Bz and the SYM-H index and the GMLAT-time plots of rTEC in four different sectors at 35°E, 75°E, 142°E, and 260°E on 7 and 8 November 2004. In Figures 5c–5f, the rTEC enhancements appear in both Japan (morning to afternoon) and North America (afternoon to night) during the main phase, but the pattern of the rTEC variations is different between the two regions. In North America, the rTEC enhancement started at a high latitude (60°N [GMLAT]) and the enhanced region moved equatorward to 20°N (GMLAT) within 4 hr, while that in Japan started at a low latitude (20–27° [GMLAT]). In central Asia (postmidnight to pr-noon) and Europe (nighttime), such rTEC enhancements cannot be seen during the main phase. At nearly the same time as the onset of the recovery phase, the large rTEC enhancement at low latitudes (20–35°N [GMLAT]) suddenly disappeared in North America. The rTEC variation in

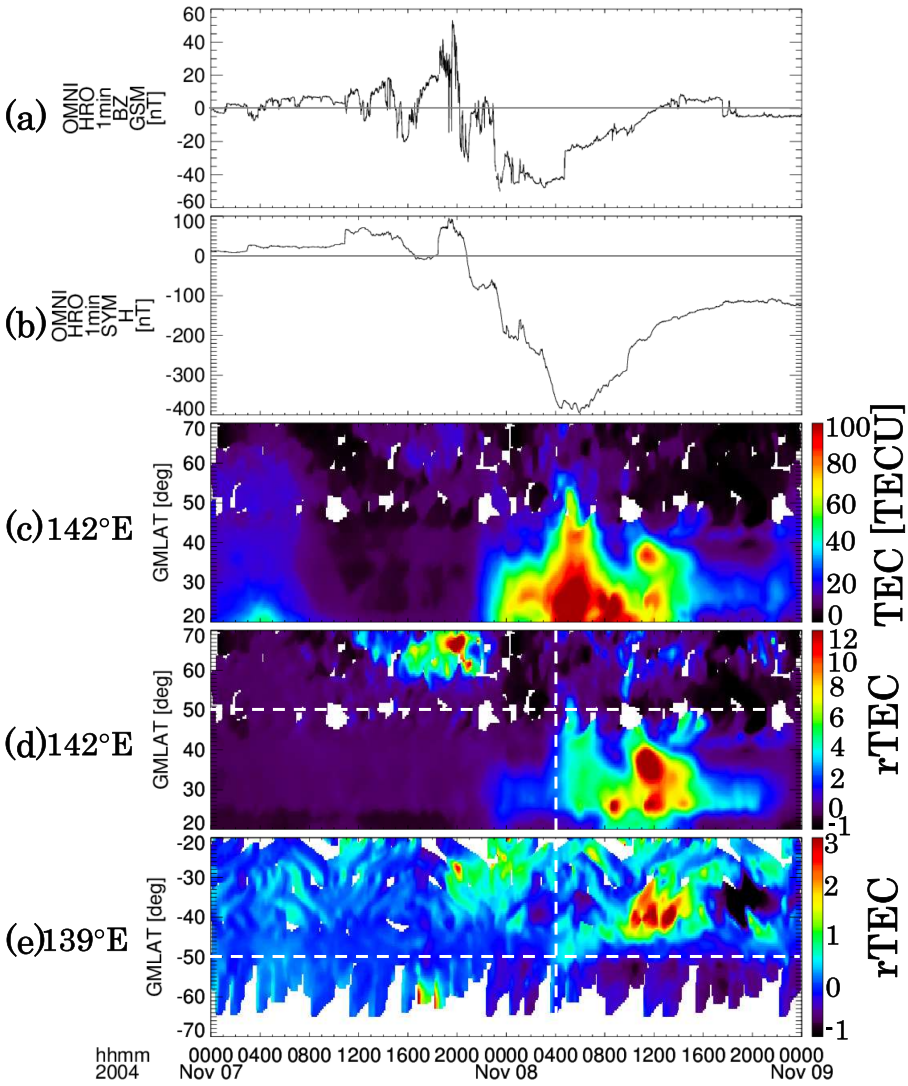

Figure 6. Time series plots of (a) interplanetary magnetic field Bz and (b) SYM-H and GMLAT-time plots of (c) TEC, (d) rTEC at 142°E and 20–70°N (GMLAT), and (e) at 139°E and -70–-20°N (GMLAT) on 7 and 8 November 2004. The color codes of the plots indicate TEC and rTEC, respectively. TECU in panel (c) indicates total electron content units (1 TECU = 10^{16}/m^2). The horizontal and vertical broken lines in panels (d) and (e) indicate 50° (GMLAT) and the onset time of the rTEC enhancements in both hemispheres, respectively.

Japan during this period will be described in detail later and shown in Figure 6. During the late recovery phase, rTEC enhancement appeared at midlatitudes (30–48°N [GMLAT]) in central Asia (Figure 6d). In Europe, rTEC enhancement did not occur at middle or low latitudes even during the recovery phase.

To investigate the temporal and spatial variations of rTEC in Japan in detail, we created a GMLAT-time plot of TEC and rTEC at a longitude of 142°E on 7 and 8 November 2004 (Figure 6). Figures 6c and 6d show the variations in TEC and rTEC at 20–70°N (GMLAT), respectively. As shown in Figure 6c, the TEC enhancement started in the low latitudes (<35°N) at 22:00 UT on 7 November 2004, during the main phase of the geomagnetic storm. At this time, the IMF Bz had a small positive value (0–5 nT) in Figure 6a. The other TEC enhancement with a latitudinally narrow structure within ~5° appeared at 58°N (GMLAT) at approximately 04:00 UT on 8 November after the IMF Bz was directed strongly southward, as shown in Figure 6a. The TEC enhancement propagated from high to low latitudes (58°N to 40°N [GMLAT]) within 3 hr. Thereafter, a TEC

reduction was seen at 33–44°N (GMLAT) between 08:00 and 10:00 UT on 8 November. At 10:30 UT on 8 November, a high-latitude TEC enhancement occurred again at 35–45°N (GMLAT) and propagated to lower latitudes. During this period, the IMF Bz showed a gradual increase from −20 to 0 nT and its direction turned northward after 12:00 UT on 8 November. As shown in Figure 6d, the rTEC variation showed nearly the same behavior as the TEC variation, but the rTEC value during 11:00–12:00 UT on 8 November increased greatly in the high latitudes (30–40°N [GMLAT]), reaching a value of more than 12.0.

To investigate the magnetic conjugacy of the rTEC enhancements in both the Northern and Southern Hemispheres, we calculated the magnetic conjugate points using the International Geomagnetic Reference Field model and compared two GMLAT-time plots of rTEC in between Japan and Australia corresponding to the magnetic conjugate regions. For this analysis, we selected two points where TEC enhancements were observed at 05:30and 11:30 UT on 8 November in the high latitudes over Japan. The locations of (48.00°N, 141.67°E) and (45.42°N, 141.67°E) in geographic latitude and longitude correspond to the magnetic conjugate points of (−30.63°N, 138.28°E) and (−28.23°N, 138.66°E), respectively. Figure 6e shows GMLAT-time plots of rTEC at 139°E and −70°N to −20°N (GMLAT) on 7 and 8 November. As shown in Figures 6d and 6e, the rTEC enhancements in Japan and Australia started at approximately 04:00 UT at 50° (GMLAT) and propagated from high to low latitudes. The high rTEC regions at approximately 11:00 UT appeared at 40° (GMLAT) in both hemispheres. This result indicates that the rTEC enhancements observed in Japan and Australia appeared with magnetic conjugacy. Furthermore, the rTEC enhancements were much larger in the Northern Hemisphere than those in the Southern Hemisphere and had different spatial structures. The different variations of the rTEC enhancements between the Northern and Southern Hemispheres do not correspond to the pattern of the IMF Bz variation.

3.4. Global Distribution of the Storm Time Variation of Neutral Composition Ratio

Figure 7 shows the global distribution of the GUVI O/N_2 ratio as a function of geographic latitude and longitude on 7 and 8 November 2004 to illustrate the global change in neutral composition ratio during the geomagnetic storm. In Figure 7a, the O/N_2 ratio is higher in the Northern Hemisphere than in the Southern Hemisphere during the geomagnetically quiet period. In Figure 7b, a large enhancement of the O/N_2 ratio can be seen in the low-latitude region from West Asia to the Pacific Ocean. Especially, the O/N_2 ratio reached a maximum around Japan. However, the O/N_2 ratio is much smaller in the Southern Hemisphere than in the Northern Hemisphere. The observed time over Japan was 05:30 UT on 8 November, corresponding to the main phase of the geomagnetic storm. Moreover, the spatial distribution of the composition ratio became symmetric about the geomagnetic equator after 11:00 UT on 8 November, corresponding to the recovery phase of the geomagnetic storm.

3.5. Comparison Between DMSP Electron Density and GNSS-TEC Data

Because there are no GNSS-TEC data over the Pacific Ocean, we compare DMSP electron density data with TEC data to investigate electron density variations in the ionosphere over the sea. Figure 8 shows a polar map of TEC in the Northern Hemisphere as a function of geomagnetic longitude and latitude at 05:50 UT during the late main phase of the geomagnetic storm on 8 November 2004 and the electron density along each DMSP satellite orbit. The TEC enhancements appeared at 40–50°N (GMLAT) over Japan and the TEC value decreased with increasing geomagnetic latitude above 50°N (GMLAT). In the westside of the American sector, the TEC-enhanced region was observed at 20–40°N (GMLAT) and a depressed TEC region appeared at 40–50°N (GMLAT). The low TEC region corresponds to the middle-latitude trough. The electron density data from DMSP satellites showed electron density enhancements between 40°N and 50°N (GMLAT) on all the satellite orbits.

Figure 9 shows the time series plots of electron temperature, electron density, and horizontal ion drift velocity observed by each satellite. In Figure 9a, the high electron density observed by F-13 in low latitudes decreased as the satellite moved into higher latitudes and the electron density gradually increased again. Moreover, the electron density decreased sharply at 05:43 UT in the middle-latitude region (48°N [GMLAT]), corresponding to the maximum value of electron temperature and increasing westward ion drift velocity. In Figures 9b and 9c, similar patterns of the electron density, temperature, and ion drift velocity variations were also observed by the F-15 and F-16 satellites, and the electron density decreased sharply at 05:54 and 05:56 UT in the middle-latitude region (45°N and 46°N [GMLAT]), respectively.

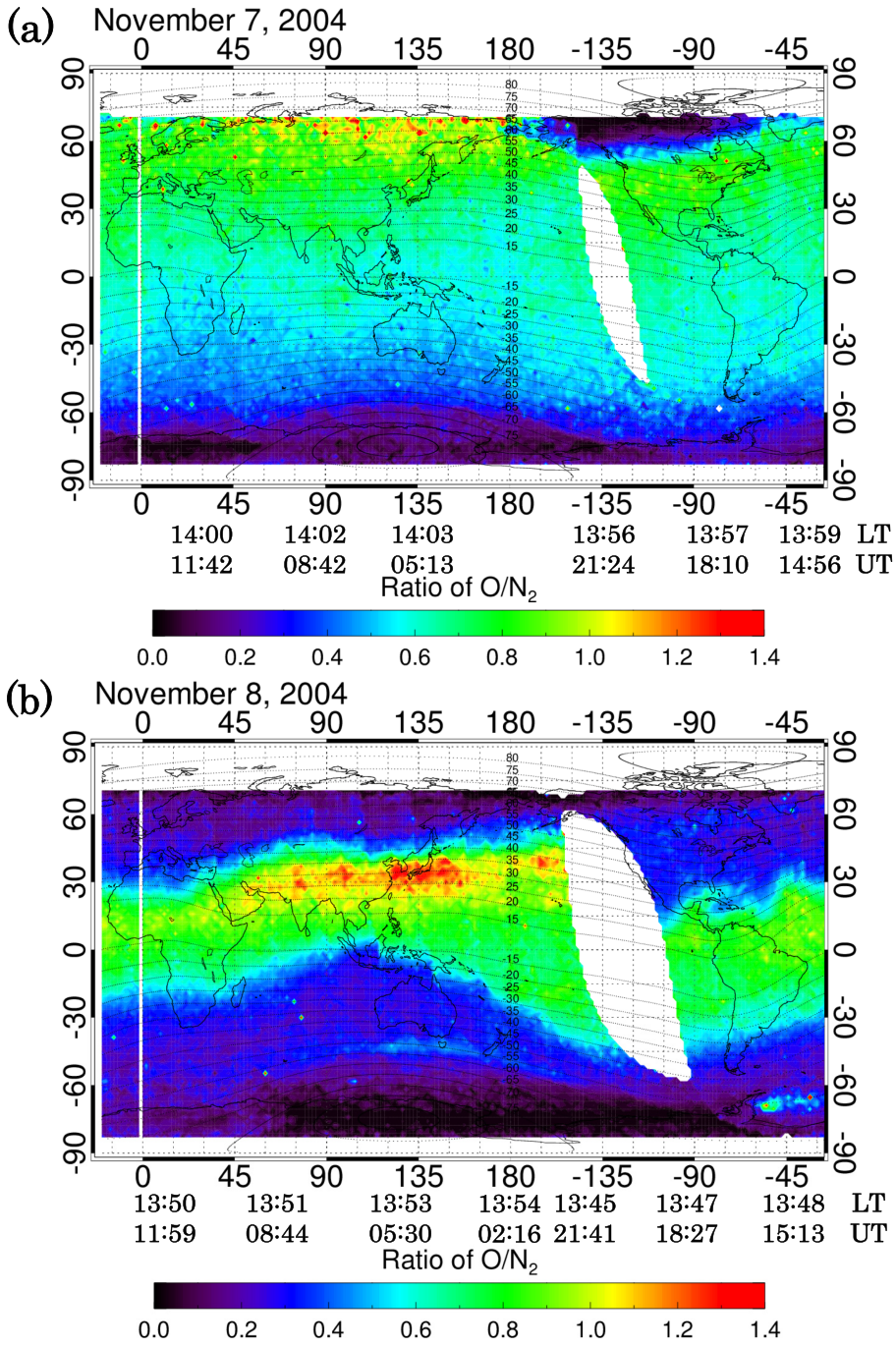

Figure 7. Global distribution of the Global Ultraviolet Imager O/N_2 ratio on (a) 7 November and (b) 8 November 2004. The color code represents the value of the O/N_2 ratio within a range from 0.0 to 1.4. The dotted curves and the numbers at 180°E indicate the magnetic latitude at a height of 300 km calculated using the Altitude-Adjusted Corrected GeoMagnetic model. Local and universal times correspond to each geographical longitude.

3.6. Storm Time Neutral Wind Variations in the Thermosphere Over Japan

Finally, we show the characteristics of neutral wind variations in the thermosphere around 300 km observed by the FPI at Shigaraki (34.8°N, 136.1°E) associated with the geomagnetic storm because this information is important for understanding the generation mechanism of the middle-latitude TEC enhancement. Figure 10

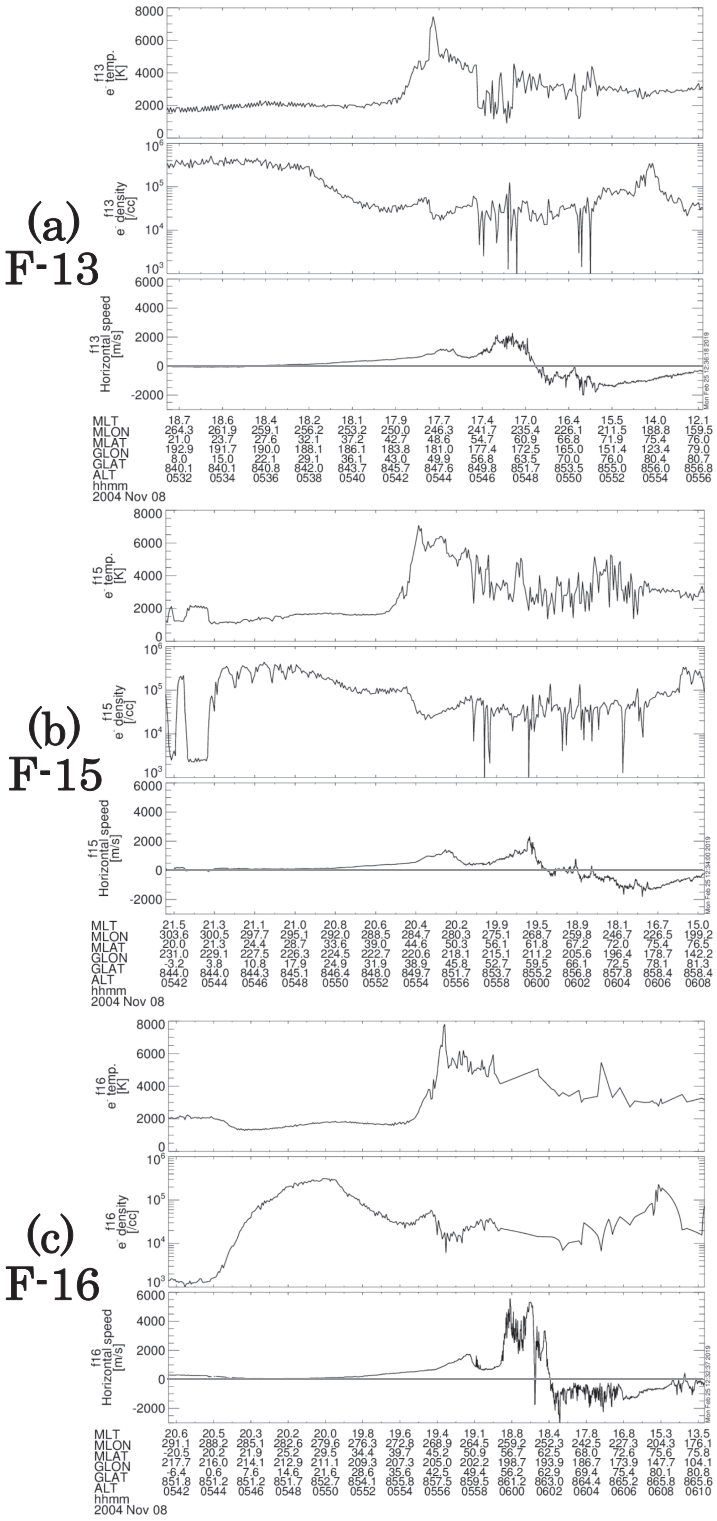

Figure 8. Global navigation satellite system-total electron content polar map as a function of geomagnetic longitude and latitude at 15–90°N (GMLAT) at 05:50 UT on 8 November 2004 and electron density data along each Defense Meteorological Satellite Program (DMSP) satellite path (F-13, F-15, and F-16) around 05:50 UT. The left and right color codes indicate global navigation satellite system-total electron content and electron density values observed by the DMSP satellites. The geomagnetic latitude lines are plotted at every 10°. Triangles on the paths indicate each DMSP satellite location at 05:50 UT. Black arrows in the dusk sector show the middle-latitude trough locations observed by the DMSP satellites.

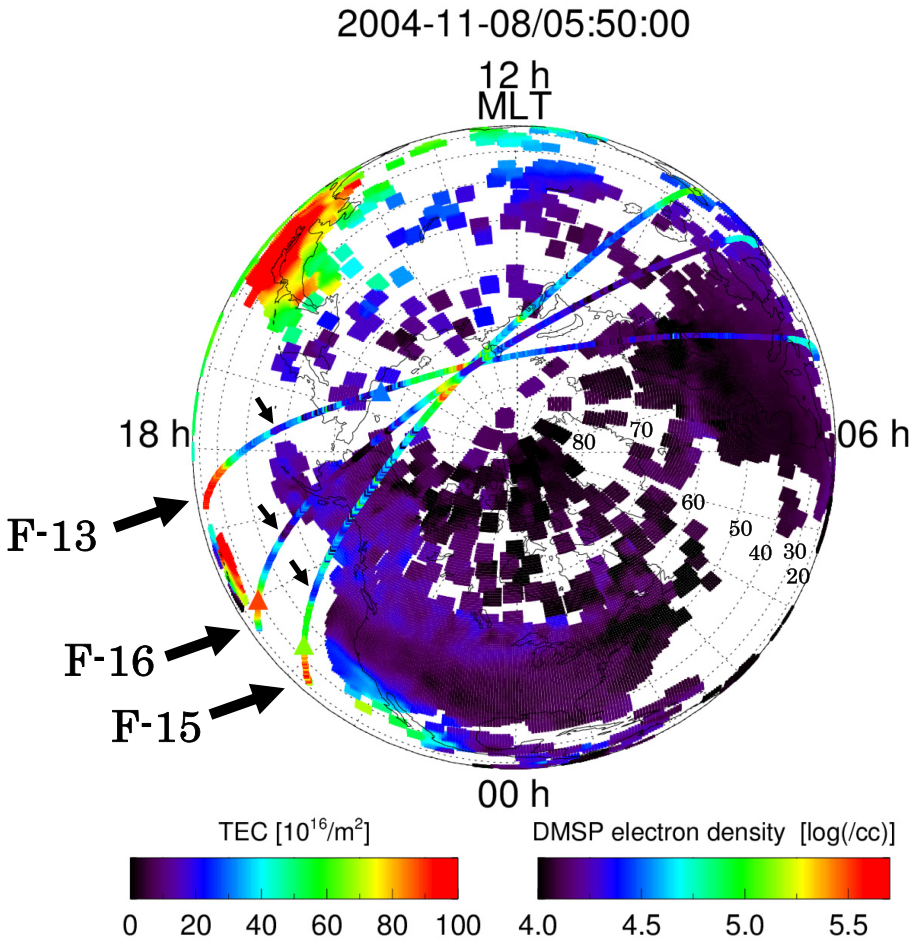

Figure 9. Time series plots of electron temperature, electron density, and horizontal ion drift velocity observed by each DMSP satellite ([a] F-13, [b] F-15, and [c] F-16). A positive value of horizontal speed represents westward velocity. TEC = total electron content; DMSP = Defense Meteorological Satellite Program.

shows time series plots of the IMF Bz, the SYM-H index, and the northward and eastward thermospheric winds on 6–9 November 2004. In Figures 10c and 10d, the northward neutral wind turned from northward to southward at around 12:00 UT on 6 November, while the eastward neutral wind remained eastward during 09:00–16:00 UT on 6 November, corresponding to geomagnetically quiet conditions. During the initial phase of the geomagnetic storm on 7 November, the patterns of the northward and eastward neutral wind variations resembled those on the previous day. However, during the recovery phase of the geomagnetic storm on 8 November, the patterns of the neutral wind variations were drastically changed. The northward neutral wind blew southward at a speed of 150 m/s at 10:00 UT, turned northward at 12:00 UT, and then reached a maximum value of 60 m/s at 15:00 UT. The eastward neutral wind turned westward during 09:00–16:00 UT and the maximum amplitude was 100 m/s at 11:00 UT.

4. Discussion

Although there have been several studies regarding TEC variation during the geomagnetic storm event that occurred on 7 and 8 November 2004, they were focused on the storm time TEC variation only at a regional scale, over North America (Basu et al., 2008), Japan (Maruyama, 2006; Balan et al., 2009; 2010), India (Dashora and Pandey, 2007; Simi et al., 2013), and South America (Fejer et al., 2007). Therefore, the global

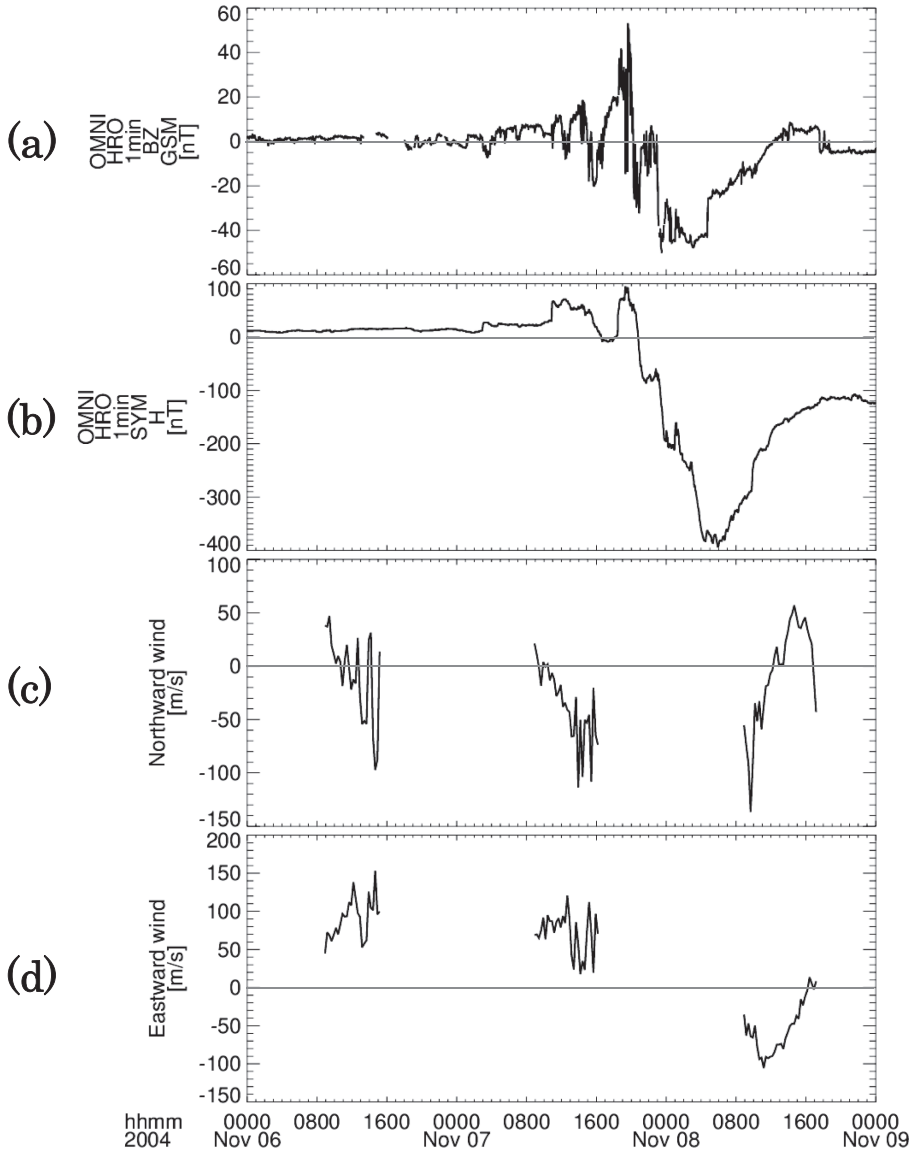

Figure 10. Time series plots of (a) interplanetary magnetic field Bz, (b) SYM-H, and (c) northward and (d) eastward neutral winds observed by Fabry-Perot interferometer at Shigaraki on 6–9 November 2004.

features of the storm time TEC variations for this event remained unknown. In this study, we analyzed the global GNSS-TEC data with high time and spatial resolution obtained from many regional GNSS networks throughout the world. As shown in Figures 2–4, we found that the rTEC enhancements first occurred in the midlatitudes over Europe, North America, and Japan during the initial and main phases of the geomagnetic storm on 7 and 8 November. The occurrence of the rTEC enhancements over North America and Japan corresponds to the periods of the southward IMF Bz, as shown in Figure 1b. Furthermore, the GUVI O/N_2 ratio observations (Figure 7a) did not show a clear enhancement of the O/N_2 ratio in North America where the rTEC enhancement was observed in the middle-latitude region after 17:00 UT on 7 November. This implies that the rTEC enhancement was not caused by a change in the neutral composition. Furthermore, as shown in Figure 10c, no significant change in the neutral wind properties in the thermosphere was found between the geomagnetically quiet day (6 November) and the initial phase of the geomagnetic storm (7 November). This indicates that the rTEC enhancement in North America after 17:00 UT on 7 November was not caused

by a storm time enhanced equatorward neutral wind, assuming that the longitudinal distribution of the meridional neutral wind was uniform. Therefore, it can be considered that the middle-latitude rTEC enhancements may have been caused by a significant enhancement of ionospheric convection due to the southward IMF Bz (e.g., Tsurutani et al., 2006). The enhanced convection electric field penetrates into the equatorial ionosphere and causes the super equatorial fountain (e.g., Tsurutani et al., 2004). However, as shown in Figures 2 and 3, the rTEC variations associated with the equatorial fountain could not be clearly identified in the equatorial and low-latitude regions of the American sector when the middle-latitude rTEC enhancements were observed. Therefore, it can be considered that the equatorial fountain effect did not contribute to the formation of the middle-latitude rTEC enhancements. On the other hand, the two rTEC enhancements over North America rapidly expand in the longitudinal direction within 1 hr and had a wide longitudinal extent (at least 75°; Figures 2f, 2g, 3b, and 3c). The enhanced rTEC region observed after 20:00 UT on 7 November is thought to extend over Pacific Ocean and to reach the Japanese sector (e.g., Figure 4c). In Figures 8 and 9, we compare DMSP electron density data with TEC data to verify the existence of the enhanced TEC region over Pacific Ocean. As shown in Figure 9, the DMSP satellite observation data indicate a significant decrease in electron density associated with the enhancement of electron temperature and westward ion drift velocity in the middle-latitude region (45–48°N [GMLAT]) around 05:50 UT on 8 November. These observations are consistent with the density, temperature, and velocity variations related to the middle-latitude trough and SAPS (e.g., Watanabe et al., 1989; Basu et al., 2008). On the contrary, electron density enhancements at the equatorward boundary of the middle-latitude trough were observed by DMSP satellites. At this time, the electron temperatures associated with the electron density enhancements were relatively low than those in the middle-latitude trough. The decrease in electron temperature is consistent with one of the features of the SED phenomenon (Liu et al., 2015, 2016a). These satellite observation data also indicate that the electron density enhancements below the equatorward boundary of the middle-latitude trough are consistent with the TEC variations in Japan and North America shown in Figure 8. Moreover, Maruyama (2006) noted that the large TEC enhancement around 12:00 UT was related to the SED phenomena. However, the present study showed that another TEC enhancement having a peak value at 45°N (GMLAT) was observed during the period 05:00–07:00 UT (Figure 6c). As shown in this panel, the TEC enhancement started at a high-latitude (~60°N [GMLAT]) and moved equatorward within 2–3 hr. This feature resembles the pattern of TEC enhancement at high latitude during 11:00–12:00 UT on 8 November and can also be categorized as an SED phenomenon. This point had not yet been clarified by Maruyama (2006).

According to previous studies regarding the characteristics of the SED phenomenon, it is known that SED tends to appear with a magnetic conjugacy in both the Northern and Southern Hemispheres (Foster and Rideout, 2007). Given this, it is suggested that TEC enhancement tends to appear in the Southern Hemisphere, corresponding to the SED phenomena observed in Japan. In fact, the present study showed that rTEC enhancements appeared in both Japan and Australia, as shown in Figures 6d and 6e. Therefore, the rTEC enhancements indicate an aspect of the SED features. However, as shown in Figures 6d and 6e, the amplitude of the rTEC in Japan was 4 times larger than that in Australia. This difference between Japan and Australia is caused by a north-south asymmetry in the neutral composition ratio (O/N_2). In fact, the GUVI O/N_2 ratio data from 8 November in Figure 7 show that the maximum value of the O/N_2 ratio in Japan at approximately 05:30 UT was more than 1.4, while the corresponding value in Australia was approximately 0.3.

Several different mechanisms for the formation of the SED structure in middle- and low-latitude regions have been proposed by many studies (e.g., Anderson, 1976; Kelley et al., 2004; Tsurutani et al., 2004; Foster et al., 2007; Zou et al., 2014; Liu et al., 2016b). Tsurutani et al. (2004) and Kelley et al. (2004) mentioned that an extension of EIA to the midlatitudes because of an enhancement in the storm time equatorial fountain effect and ambipolar diffusion along the magnetic field line mainly contribute to SED formation. Foster et al. (2007) further noted that the westward transport of a high-latitude portion of EIA because of the storm time-enhanced SAPS is a result of the SED plume. However, the enhanced rTEC region over North America at 20:00 UT on 7 November directly formed across North America with a wide longitudinal extent of more than 75° within 1 hr, although the rTEC enhancement related to the equatorial fountain effect could not be found in the equatorial and low-latitude regions, as shown in Figures 3b and 3c. This

observational fact suggests that the origin of the SED phenomenon is not the westward transport of a higher portion of the EIA due to the SAPS electric field (Foster et al., 2007).

From the above discussion, we can infer that an enhanced rTEC region with an SED nature was formed in between North America and Japan with a longitudinal extent of more than 100°. Moreover, as shown in Figures 4i, 5d, and 5e, a region of rTEC enhancement appeared in central Asia after 11:00 UT on 8 November simultaneously with the largest rTEC value observed in Japan. Therefore, we can also suggest that an rTEC-enhanced region with an SED feature occurred in between Japan and central Asia with a longitudinal extent of ~70°. Liu et al. (2016b) pointed out that local upward $\mathbf{E} \times \mathbf{B}$ ion drifts are most important in generating the SED in the topside ionosphere. Therefore, we can infer that storm time electric fields are distributed simultaneously over a wide longitudinal sector and generate such a longitudinally wide SED structure. This hypothesis should be proved by analyzing ionospheric electric field observations together with global TEC data in a future study.

Finally, we compare the longitudinal extent of the SED plume reported by several previous studies with that observed in the present study. Foster and Rideout (2007) and Coster et al. (2007) showed several two-dimensional TEC maps depicting SED structures during three large geomagnetic storms. From these maps, we determined the longitudinal width of the SED structure as 20–40°. Zou et al. (2013) investigated the TEC variations during a geomagnetic storm on 24 and 25 October 2011. The SED plume was observed at 01:45–01:50 UT with a longitudinal extent of 30°. In this study, we found that the SED structure had a wide longitudinal width (~100°) during the geomagnetic storm. Therefore, the longitudinal extent of this SED event is 2.5–5.0 times longer than those reported in previous studies.

5. Conclusions

To investigate the characteristics of electron density variations in the ionosphere during a geomagnetic storm that occurred on 7 and 8 November 2004, we analyzed global TEC variations using global GNSS-TEC data together with solar wind, IMF, geomagnetic indices, electron density, temperature, and ion drift velocity data collected by DMSP satellites and thermospheric neutral wind data obtained from FPI at Shigaraki. As a result of this analysis, we found that enhanced TEC regions over North America and Europe first appeared in the middle-latitude regions during the initial and main phases of the geomagnetic storm. The TEC-enhanced regions over North America showed a rapid longitudinal expansion within 1 hr and reached a wide longitudinal extent. Regions of TEC enhancement were also observed in Japan. Observation data from the DMSP showed a slight enhancement of the electron density at 850 km below the equatorward boundary of the middle-latitude trough (45–48°N in geomagnetic latitude) over the Pacific Ocean. This electron density enhancement may correspond to the TEC enhancements observed in both Japan and North America. These results imply that a TEC-enhanced region existed between North America and Japan. The TEC enhancement in Japan appeared with a magnetic conjugacy in the Southern Hemisphere, indicating one of the characteristics of SED. Moreover, TEC enhancements simultaneously appeared from Japan to central Asia at 11:00 UT on 8 November, corresponding to the early recovery phase of the geomagnetic storm. From the above results, it is suggested that SED phenomena can be simultaneously generated within a wide longitudinal width (~100°). From a comparison of the longitudinal extent of the SED structures reported by previous studies and that shown by the present study, it can be concluded that the longitudinal extent of this SED event was 2.5–5.0 times longer than those reported by previous studies.

Acknowledgments
This study was supported by the Japan Society for the Promotion of Science, KAKENHI Grants 26400478, 15H05815, and 16H05736 and the Japan Society for the Promotion of Science, KAKENHI Grant 16H06286. The coauthor (A. S.) was also supported by the National Institute of Polar Research through General Collaboration Project 29-11. We used IUGONET products to analyze the GNSS-TEC data and other data sets. We used geomagnetic indices and a list of geomagnetically quiet and disturbed days provided by the World Data Center (WDC) for Geomagnetism, Kyoto University (http://wdc.kugi.kyoto-u.ac.jp/index.html). The solar wind and IMF data were provided by NASA's CDAWeb (https://cdaweb.sci.gsfc.nasa.gov/index/.html). The GNSS data collection and processing were performed using the National Institute of Information and Communications Technology Science Cloud. The GUVI data used here were provided through support from the NASA MO&DA program. The GUVI instrument was designed and built by The Aerospace Corporation and The Johns Hopkins University. The Principal Investigator is Dr. Andrew B. Christensen, and the Chief Scientist and co-PI is Dr. Larry J. Paxton.

References

Abdu, M. A. (1997). Major phenomena of the equatorial ionosphere-thermosphere system under disturbed conditions. *J. Atmospheric Solar Terrest. Phys.*, *59*, 1505–1519.

Anderson, D. N. (1976). Modeling the midlatitude F-region ionospheric storm using east-west drift and a meridional wind. *Planet. Space Sci.*, *24*, 69–77. https://doi.org/10.1016/0032-0633(76)90063-5

Balan, N., Alleyne, H., Otsuka, Y., Vijaya, L. D., Fejer, B. G., & McCrea, I. (2009). Relative effects of electric field and neutral wind on positive ionospheric storms. *Earth Planets Space*, *61*(4), 439–445.

Balan, N., Shiokawa, K., Otsuka, Y., Kikuchi, T., Vijaya Lekshmi, D., Kawamura, S., et al. (2010). A physical mechanism of positive ionospheric storms at low and mid latitudes through observations and modeling. *J. Geophys. Res.*, *115*, A02304. https://doi.org/10.1029/2009JA014515

Basu, Su., S. Basu, J. J. Makela, E. MacKenzie, P. Doherty, J. W. Wright, et al., and A. J. Coster (2008), Large magnetic storm-induced nighttime ionospheric flows at midlatitudes and their impacts on GPS-based navigation systems, *J. Geophys. Res.*, **113**, A00A06, doi:10.1029/2008JA013076.

Buonsanto, M. J. (1999). Ionospheric storms—A review. *Space Sci. Rev.*, *88*(3–4), 63–601. https://doi.org/10.1023/A:1005107532631

Coster, A. J., Foster, J. C., & Erickson, P. J. (2003). Monitoring the ionosphere with GPS. *GPS World*, *14*, 40.

Coster, A. J., Colerico, M. J., Foster, J. C., Rideout, W., & Rich, F. (2007). Longitude sector comparisons of storm enhanced density. *Geophys. Res. Lett.*, *34*, L18105. https://doi.org/10.1029/2007GL030682

Dashora, N., & Pandey, R. (2007). Variations in the total electron content near the crest of the equatorial ionization anomaly during the November 2004 geomagnetic storm. *Earth Planets Space*, *59*, 127–131.

Fagundes, P. R., Cardoso, F. A., Fejer, B. G., Venkatesh, K., Ribeiro, B. A. G., & Pillat, V. G. (2016). Positive and negative GPS-TEC ionospheric storm effects during the extreme space weather event of March 2015 over the Brazilian sector, *J. Geophys. Res. Space Physics*, *121*, 5613–5625. https://doi.org/10.1002/2015JA022214

Fejer, B. G., Jensen, J. W., Kikuchi, T., Abdu, M. A., & Chau, J. L. (2007). Equatorial ionospheric electric fields during the November 2004 magnetic storm. *J. Geophys. Res.*, *112*, A10304. https://doi.org/10.1029/2007JA012376

Foster, J. C. (1993). Storm-time plasma transport at middle and high latitudes. *J. Geophys. Res.*, *98*, 1675–1689. https://doi.org/10.1029/92JA02032

Foster, J. C., & Vo, H. B. (2002). Average characteristics and activity dependence of the subauroral polarization stream. *Journal of Geophysical Research*, *107*(A12), 1475. https://doi.org/10.1029/2002JA009409

Foster, J. C., Rideout, W., Sandel, B., Forrester, W. T., & Rich, F. J. (2007). On the relationship of SAPS to storm enhanced density. *Journal of Atmospheric Space Terrestrial Physics*, *69*(3), 303–313. https://doi.org/10.1016/j.jastp.2006.07.021

Foster, J. C., & Rideout, W. (2007). Storm enhanced density: Magnetic conjugacy effects. *Ann. Geophys.*, *25*, 1791–1799.

Fuller-Rowell, T. J., Codrescu, M. V., Moffett, R. J., & Quegan, S. (1994). Response of the thermosphere and ionosphere to geomagnetic storms. *J. Geophys. Res.*, *99*(A3), 3893–3914.

Fuller-Rowell, T. J., Codrescu, M. V., Roble, R. G., & Richmond, A. D. (1997). How does the thermosphere and ionosphere react to a geomagnetic storm? In B. T. Tsurutani, W. D. Gonzales, Y. Kamide, & J. K. Arballo (Eds.), *Magnetic Storms, Geophysical Monograph 98*. 203–225. Washington, DC: American Geophysical Union.

Hayashi, H., Y. Koyama, T. Hori, Y. Tanaka, S. Abe, A. Shinbori, et al., T. Motoba and IUGONET project team (2013), Inter-university Upper Atmosphere Global Observation NETwork (IUGONET), *Data Sci. J.*, **12**, WDS179-WDS184, doi: 10.2481/dsj. WDS 030, 2013

Jakowski, N., E. Sardon, E. Engler, A. Jungstand, and D. Klähn (1996), Relationships between GPS-signal propagation errors and EISCAT observations. *Annales Geophysicae*, *European Geosciences Union*, **14**(12), 1429–1436. <hal-00316269>

Kelley, M. C., Vlasov, M. N., Foster, J. C., & Coster, A. J. (2004). A quantitative explanation for the phenomenon known as storm-enhanced density. *Geophys. Res. Lett.*, *31*, L19809. https://doi.org/10.1029/2004GL020875

Liu, J., Nakamura, T., Liu, L., Wang, W., Balan, N., Nishiyama, T., et al. (2015). Formation of polar ionospheric tongue of ionization during minor geomagnetic disturbed conditions, *J. Geophys. Res. Space Physics*, *120*, 6860–6873. https://doi.org/10.1002/2015JA021393

Liu, J., Wang, W., Burns, A., Yue, X., Zhang, S., Zhang, Y., & Huang, C. (2016a). Profiles of ionospheric storm-enhanced density during the 17 March 2015 great storm, *J. Geophys. Res. Space Physics*, *121*, 727–744. https://doi.org/10.1002/2015JA021832

Liu, J., Wang, W., Burns, A., Solomon, S. C., Zhang, S., Zhang, Y., & Huang, C. (2016b). Relative importance of horizontal and vertical transports to the formation of ionospheric storm-enhanced density and polar tongue of ionization, *J. Geophys. Res. Space Physics*, *121*, 8121–8133. https://doi.org/10.1002/2016JA022882

Lin, C. H., Richmond, A. D., Heelis, R. A., Bailey, G. J., Lu, G., Liu, J. Y., et al. (2005). Theoretical study of the low- and midlatitude ionospheric electron density enhancement during the October 2003 superstorm: Relative importance of the neutral wind and the electric field. *J. Geophys. Res.*, *110*, A12312. https://doi.org/10.1029/2005JA011304

Mannucci, A. J., B. T. Tsurutani, B. A. Iijima, A. Komjathy, A. Saito, W. D. Gonzalez, et al., and R. Skoug (2005), Dayside global ionospheric response to the major interplanetary events of October 29–30, 2003 "Halloween Storms," *Geophys. Res. Lett.*, **32**, L12S02, doi:10.1029/2004GL021467.

Maruyama, T. (2006). Extreme enhancement in total electron content after sunset on 8 November 2004 and its connection with storm enhanced density. *Geophys. Res. Lett.*, *33*, L20111. https://doi.org/10.1029/2006GL027367

Matsushita, S. (1959). A study of the morphology of ionospheric storms. *J. Geophys. Res.*, *13*, 305–321.

Matuura, N. (1972). Theoretical models of ionospheric storms, *Space Sci. Rev.*, *13*, 124–189.

Otsuka, Y., Ogawa, T., Saito, A., Tsugawa, T., Fukao, S., & Miyazaki, S. (2002). A new technique for mapping of total electron content using GPS network in Japan. *Earth, Planets and Space*, *54*(1), 63–70. https://doi.org/10.1186/BF03352422

Prölss, G. W. (1997). Magnetic storm associated perturbations of the upper atmosphere. In B. T. Tsurutani, W. D. Gonzales, Y. Kamide, & J. K. Arballo (Eds.), *Magnetic Storms, Geophysical Monograph 98*. 227–241. Washington, DC: American Geophysical Union.

Rees, D. (1996). Observations and modelling of ionospheric and thermospheric disturbances during major geomagnetic storms: A review. *J. Atmospheric Terrest. Phys.*, *57*, 1433–1457.

Schunk, R. W., & Sojka, J. J. (1996). Ionosphere-Thermosphere Space Weather Issues. *J. Atmospheric Terrest. Phys.*, *58*, 1527–1574.

Shepherd, S. G. (2014). Altitude-adjusted corrected geomagnetic coordinates: Definition and functional approximations. *Journal of Geophysical Research: Space Physics*, *119*, 7501–7521. https://doi.org/10.1002/2014JA020264

Shinbori, A., Otsuka, Y., Tsugawa, T., Nishioka, M., Kumamoto, A., Tsuchiya, F., et al. (2018). Temporal and spatial variations of storm time midlatitude ionospheric trough based on global GNSS-TEC and Arase satellite observations. *Geophysical Research Letters*, *45*, 7362–7370. https://doi.org/10.1029/2018GL078723

Shiokawa, K., Kadota, T., Otsuka, Y., Ogawa, T., Nakamura, T., Tsuda, T., & Fukao, S. (2003). A two-channel Fabry-Perot interferometer with cooled-CCD detectors for neutral wind measurement in the upper atmosphere. *Earth Planets Space*, *55*, 271–275.

Simi, K. G., Manju, G., Madhav Haridas, M. K., Prabhakaran Nayar, S. R., Pant, T. K., & Alex, S. (2013). Ionospheric response to a geomagnetic storm during November 8–10, 2004. *Earth Planets Space*, *65*, 343–350.

Spiro, R. W., Wolf, R. A., & Fejer, B. G. (1988). Penetration of high-latitude-electric-field effects to low latitudes during SUNDIAL 1984. *Ann. Geophys.*, *6*, 39–50.

Tanaka, Y., Shinbori, A., Hori, T., Koyama, Y., Abe, S., Umemura, N., et al. (2013). Analysis software for upper atmospheric data developed by the IUGONET project and its application to polar science. *Adv. Polar Sci.*, *24*, 231–240. https://doi.org/10.3724/SP.J.1085.2013.00231

Thebault, E., Finlay, C. C., Beggan, C. D., Alken, P., Aubert, J., Barrois, O., et al. (2015). International geomagnetic reference field: The 12th generation. *Earth, Planets and Space*, *67*, 79. https://doi.org/10.1186/s40623-015-0228-9

Thomas, E. G., Baker, J. B. H., Ruohoniemi, J. M., Clausen, L. B. N., Coster, A. J., Foster, J. C., & Erickson, P. J. (2013). Direct observations of the role of convection electric field in the formation of a polar tongue of ionization from storm enhanced density. *J Geophys Res Space Physics*, *118*, 1180–1189. https://doi.org/10.1002/jgra.50116

Tsugawa, T., Kotake, N., Otsuka, Y., & Saito, A. (2007). Medium-scale traveling ionospheric disturbances observed by GPS receiver network in Japan: A short review. *GPS Solutions*, *11*(2), 139–144. https://doi.org/10.1007/s10291-006-0045-5

Tsugawa, T., Nishioka, M., Ishii, M., Hozumi, K., Saito, S., Shinbori, A., et al. (2018). Total electron content observations by dense regional and worldwide international networks of GNSS. *Journal of Disaster Research*, *13*(3), 535–545. https://doi.org/10.20965/jdr.2018.p0535

Tsurutani, B., A. Mannucci, B. Iijima, M. A. Abdu, J. H. A. Sobral, W. Gonzalez, F. Guarnieri,2 T. Tsuda, A. Saito, K. Yumoto, B. Fejer, T. J. Fuller-Rowell, J. Kozyra, J. C. Foster, A. Coster and V. M. Vasyliunas (2004), Global dayside ionospheric uplift and enhancement associated with interplanetary electric fields, *J. Geophys. Res.*, *109*, A08302, doi:https://doi.org/10.1029/2003JA010342.

Tsurutani, B. T., W. D. Gonzalez, A. L. C. Gonzalez, F. L. Guarnieri, N. Gopalswamy, M. Grande, et al. (2006), Corotating solar wind streams and recurrent geomagnetic activity: A review. *Journal of Geophysical Research*, **111**, A07S01, doi:10.1029/2005JA011273.

Watanabe, S., Oyama, K.-I., & Abe, T. (1989). Electron temperature structure around mid latitude ionospheric trough. *Planet. Space Sci.*, *37*, 1453–1460.

Yizengaw, E., Moldwin, M. B., & Galvan, D. A. (2006). Ionospheric signatures of a plasmaspheric plume over Europe. *Geophys. Res. Lett.*, *33*, L17103. https://doi.org/10.1029/2006GL026597

Zou, S., Ridley, A. J., Moldwin, M. B., Nicolls, M. J., Coster, A. J., Thomas, E. G., & Ruohoniemi, J. M. (2013). Multi-instrument observations of SED during 24–25 October 2011 storm: Implications for SED formation processes, *J. Geophys. Res. Space Physics*, *118*, 7798–7809. https://doi.org/10.1002/2013JA018860

Zou, S., Moldwin, M. B., Ridley, A. J., Nicolls, M. J., Coster, A. J., Thomas, E. G., & Ruohoniemi, J. M. (2014). On the generation/decay of the storm-enhanced density plumes: Role of the convection flow and field-aligned ion flow, *J. Geophys. Res. Space Physics*, *119*, 8543–8559. https://doi.org/10.1002/2014JA020408